Water Air Soil Pollut (2012) 223:2073–2081
DOI 10.1007/s11270-011-1005-4

One-Pot Construction of Titania-γ-AlOOH Nanocomposites Employed for Photocatalytic Degradation

Fei Chang · Min Zhang · Gang Wang · Wenjian Shi · Xuefeng Hu

Received: 21 July 2011 / Accepted: 17 October 2011 / Published online: 11 November 2011

Abstract A series of aluminum oxyhydroxide-incorporated titania composites were prepared by a one-pot synthetic procedure using aluminum tri-*sec*-butoxide as a precursor. The as-synthesized samples were characterized by Fourier transform infrared spectrophotometer, X-ray diffraction, thermogravimetry and differential scanning calorimetry, nitrogen physisorption, and scanning electron microscopy. It was identified that aluminum oxyhydroxide (γ-AlOOH, or boehmite) was produced as aluminum matrix into which titania, commercially available P25, was incorporated. Photocatalytic activity of all nanocomposites was evaluated with respect to the photodecolorization of methyl orange under UV irradiation and almost complete decolorization was eventually achieved under optimum experimental conditions.

Keywords Photocatalytic · Nanocomposites · γ-AlOOH · Methyl orange

1 Introduction

Heterogeneous photocatalysis driven by semiconductor materials has recently attracted enormous attention in terms of wastewater and air treatment since it is reliable to complete the mineralization of persistent pollutants under mild conditions (Thompson and Tates 2006). The most researched semiconductor at present is titania (TiO_2) due to its effective photocatalytic activity, long-term stability, low cost, low toxicity, and being easily available (Chong et al. 2010; Malato et al. 2009; Han et al. 2009). A practical water purification process inevitably involves a reactor containing catalyst slurry. The recovery of TiO_2 nanoparticles after degradation from the aqueous suspension is thus a main challenge. Furthermore, nanosized powders generally have a tendency of aggregation in solutions, which is detrimental to photocatalytic systems (Hoffmann et al. 1995). In addition, the relatively low photocatalytic ability was also attributed to the lack of strong adsorption of TiO_2 to pollutant compounds.

Immobilization of TiO_2 nanoparticles into supporting materials is reliable to facilitate the stabilization and filtration of photocatalysts in nanoscale, though in some occasions immobilized TiO_2 suffers low photocatalytic efficiency because of a reduced surface area

Electronic supplementary material The online version of this article (doi:10.1007/s11270-011-1005-4) contains supplementary material, which is available to authorized users.

F. Chang (✉) · M. Zhang · G. Wang · W. Shi
School of Environment and Architecture,
University of Shanghai for Science and Technology,
Shanghai 200093, People's Republic of China
e-mail: Feichang@usst.edu.cn

X. Hu (✉)
Key Laboratory of Coastal Environmental Processes,
Yantai Institute of Coastal Zone Research,
Chinese Academy of Sciences,
Yantai 264003, People's Republic of China
e-mail: xfhu@yic.ac.cn

(Jiang et al. 2011). A variety of materials have been investigated as supports for hosting TiO_2 nanoparticles, such as carbonaceous materials (Leary and Westwood 2011), glass beads (Chiou et al. 2006), ceramics (Qiu et al. 2011), zeolites (Petkowicz et al. 2010), and celluloses (Zeng et al. 2010). Besides the ease of filtration and stabilization of nanosized catalyst particles, an appropriate support bearing a large surface area is advantageous to interact with target organic pollutants and subsequently degrade them.

Boehmite has been found to have wide applications not only as absorbents and flame redundants (Kawasaki et al. 2010) but also as a general precursor for producing aluminum oxides, which are generally utilized as catalysts, ceramics, capacitors, substrates for integrate circuits, and catalyst supports (Roco 1999). With abundant hydroxyl groups, boehmite tends to interact with pollutants via the formation of hydrogen bonds, hence facilitating adsorption and further degradation. Numerous synthetic methods have been reported to obtain boehmite with controllable particle size and desired microstructures, such as sol-gel (Yang et al. 2009), hydrothermal (Arami et al. 2008), wet chemical precipitation (Panias and Krestou 2007), and spray (Caiut et al. 2009), among which one-pot direct synthesis has been recently developed to produce metal nanoparticles embedded into boehmite to catalyze hydrogenation or oxidation reactions under mild circumstances (Park et al. 2007; Chang et al. 2010). This preparation is simple and favorable to fabricate boehmite fibers with metal nanoparticles incorporated.

Though metal or metal oxides embedded into or supported on the boehmite are extensively used as catalysts or sensors, few attempts have been made to construct titania-incorporated boehmite aimed at photocatalytic evaluation. As a result, in the present study, we focused on the preparation of titania-boemite nanocomposites via one-pot synthetic method using aluminum tri-*sec*-butoxide as a precursor. After structural characterization, these samples in aqueous solution were exposed to UV irradiation to catalyze the photodegradation of methyl orange, a simulate pollutant. Several factors, which may influence the photocatalytic activity, were systematically studied. These catalysts showed satisfactory decolorization efficiency under the conditions tested. Coupled with features of easy preparation, recovery, and regeneration, these composites can be potentially employed for the photocatalyzed degradation of organic pollutants or toxic metal species in environmental protection and remediation, as well as catalysts or catalyst supports to drive organic transformations.

2 Experimental

2.1 Reagents

Aluminum tri-*sec*-butoxide (Al(O-*sec*-Bu)$_3$) was purchased from Shanghai Crystal Pure Reagent Co. Ltd., in China. Degussa P25, a commercial titania powder, was afforded by Germany Degussa corperation. Methyl orange and organic solvents, such as acetone and absolute ethanol, were obtained from Sinopharm Chemical Reagent Co. Ltd. (Shanghai, China). All the reagents of analytical grade were used without any further purification and all the aqueous solutions were prepared with deionized water.

2.2 Preparation of Titania-γ-AlOOH Nanocomposites

The P25-incorporated boehmite catalysts were prepared via a modified one-pot procedure from aluminum tri-*sec*-butoxide and Degussa P25 (Park et al. 2007). A typical synthesis was described in detail as follows: P25 (0.3 g, 3.75 mmol) and absolute ethanol (8 g) were charged into a 100-mL round-bottomed flask equipped with a condenser, into which Al(O-*sec*-Bu)$_3$ (10.9 g, 44.25 mmol) was added. The mixture was allowed to stir at 130°C for 3 h. After careful addition of 3 mL water, the mixture was aged at the same temperature for another 3 h. The P25-incorporated boehmite catalyst was finally obtained by filtration, washed with water twice and acetone once, and dried at 120°C for 2 h. The filtrates were collected and analyzed with a ICP plasma emission spectrometer, and no titanium and aluminum species were detectable. Therefore, we theoretically calculated the mass fraction of P25 as approximately 10 wt.% based upon the amount of P25 divided by the total mass of the collected product. Similarly, two other samples containing 30% and 40% mass fraction of P25 were prepared by variation of the Al(O-*sec*-Bu)$_3$ amount. They were denoted as Ti–Al-10, Ti–Al-30, and Ti–Al-40 for the sake of convenience, where 10, 30, and 40 herein refer to the mass fraction of P25,

respectively. Bare boehmite was also synthesized by using the same procedure in the absence of P25.

2.3 Characterization

Powder X-ray diffraction (XRD) patterns were recorded on a Bruker D8 Advance X-ray diffractometer with Cu Kα radiation source, at a step size of 0.02° within the range from 10° to 90° in 2θ. Infrared spectra were generated on a Bruker V-70 Fourier transform-infrared spectrophotometer using KBr pellet technique. The composition of as-synthesized specimens was conducted on a STA-449C thermogravimetry and differential scanning calorimetry (TG-DSC) instrument at a heating rate of 10° min^{-1} under nitrogen atmosphere. The sample morphology was checked by using a HITACHI S-4800 scanning electron microscopy (SEM). Nitrogen adsorption measurements were performed using an ASAP 2010 volumetric adsorption analyzer at 77 K with ultra-high purity nitrogen gas. The UV–vis adsorption spectra of the products were carried out on a Purkinje General T6 spectrophotometer (China).

2.4 Photocatalytic Experiments

Methyl orange (MO) powder was dissolved in pure water to make a stock solution of desired concentration. The pH value of MO solution was unregulated unless otherwise stated. The photocatalytic activity of the titania-γ-AlOOH nanocomposites was evaluated by batch experiments using a LIMX-VII apparatus manufactured by Bylabo Precision Instrument Co. Ltd. (Xi'an, China). Under magnetic stirring, the aqueous system containing MO and as-synthesized samples was set in the dark for 1 h to ensure the adsorption–desorption equilibrium of MO with the catalysts before exposing to UV light from a 300-W high-pressure mercury lamp with wavelength of 365 nm. The photocatalytic activity was attained through measurement of the absorbance band of MO at 464 nm after a fixed irradiation time. The absorbance measurement of reaction solutions was performed after separating the catalyst from the reaction solutions by centrifugation for 15 min (12,000 revolutions min^{-1}) and subsequent filtration through a 0.22-μm syringe filter. Each value in this study is the average of two replicate samples.

The catalyst durability was estimated according to the procedure below. After each run of degradation, the catalyst was collected from aqueous solution by centrifugation, rinsed successively with 1 M aqueous NaOH solution, deionized water, and ethanol, and dried at 80°C for 4 h. Afterwards, each recycling test was conducted under a similar condition and the consumption of MO was determined to show the variation of retained concentration.

3 Results and Discussion

3.1 X-ray Diffraction of Crystal Phases

Wide-angle X-ray diffraction patterns of commercial P25, Ti–Al-10, Ti–Al-30, and Ti–Al-40 and bare boehmite are shown in Fig. 1. Five characteristic diffraction peaks at 2θ=14.24° for (020), 27.82° for (120), 38.16° for (140), 48.78° for (200), and 64.9° for (231) are detectable and assigned to orthorhombic γ-AlOOH phase. Beyond that, the absence of peaks belonging to other phases is indicative of high purity. These broadened peaks observed imply the formation of microcrystalline boehmite and crystallite size is evaluated as around 4 nm using Scherrer's formula, similar to the size reported (Hochepied and Nortier 2002). From Fig. 1, it is obvious that with an increase of P25 content from 10 to 40 wt.%, the diffraction peaks were gradually enhanced according to pure P25

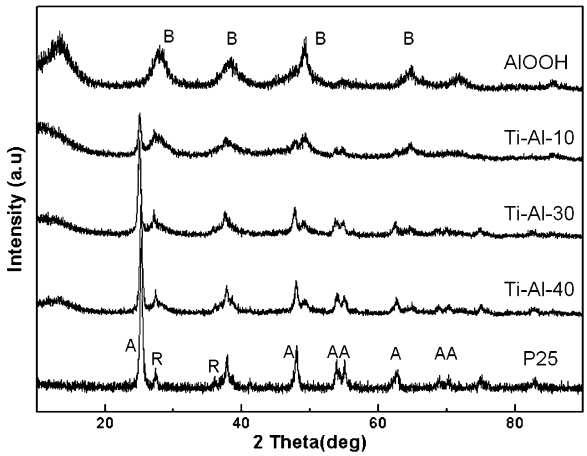

Fig. 1 XRD patterns of Ti–Al series, γ-AlOOH, and bare P25. *A*, anatase; *B*, boehmite; *R*, rutile

X-ray pattern on the bottom, signifying that P25 was successfully incorporated into the γ-AlOOH matrix.

3.2 FT-IR Analysis

The FT-IR spectra of as-synthesized Ti–Al series are given in Fig. 2. As seen in AlOOH curve, peaks at 474 and 617 cm^{-1} were generated from the octahedral coordination Al–O stretching and bending vibrations, respectively. Peaks appear at 734 and 1,070 cm^{-1} from torsional and symmetrical bending (Al)O–H vibrations. An acromion at 3,091 cm^{-1} relates to symmetrical stretching (Al)O–H vibration (Hochepied and Nortier 2002). The characteristic peaks mentioned above confirm the formation of microcrystalline boehmite in agreement with XRD results. All samples exhibit both peaks to be located at nearly 3,400–3,600 and 1,630 cm^{-1}, attributed to the stretching and bending vibration of O–H bond in adsorbed water. For the pure P25 case, the absorption bond from 400 to 900 cm^{-1} was assigned to the stretching vibration of Ti–O–Ti bond. From the spectra, we conclude that P25 has been incorporated into the boehmite phase maintaining the original microstructure. Liu et al. reported the preparation of boehmite-coated rutile TiO_2 and they found that with a decrease of the mole ratio of Al/Ti, the intensities of Al–O stretching vibration 1,070 cm^{-1} decreased but locations were red-shifted (Liu et al. 2009), which was attributed to the formation of Ti–O–Al bonds. Interestingly, with a decrease of Al content, the intensities of bands are similarly decreased without variation of their locations in our observation. However, it is quite evident that peaks at 3,091 and 474 cm^{-1}, corresponding to the symmetrical stretching (Al)O–H vibration and Al–O stretching vibration, were red-shifted after the introduction of titania, possibly owing to the interaction of Ti species with relevant H and O atoms on the surface of boehmite or the direct formation of chemical bonds.

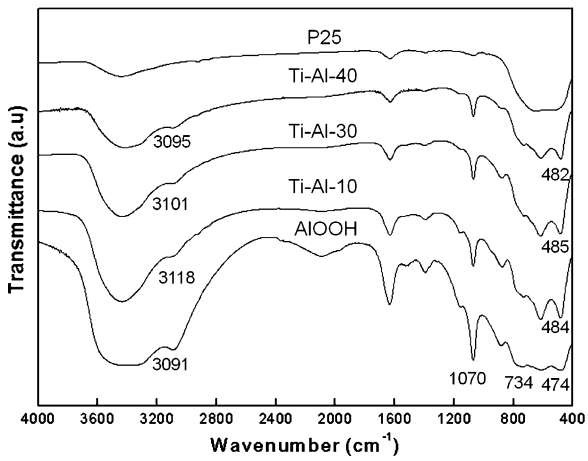

Fig. 2 FT-IR spectra of Ti–Al series, γ-AlOOH, and bare P25

3.3 Thermal Behavior Measurements

Thermal behavior of prepared nanocomposites and pure γ-AlOOH were checked and shown in Fig. 3. Figure 3a represents the weight loss of four samples at different temperatures and Fig. 3b depicts the TG-DSC analysis of pure γ-AlOOH (TG-DSC analysis for other samples is shown in Fig. S1 of the "Electronic Supplementary Materials"). As seen from Fig. 3, the mass loss of all samples with an endothermic peak centered at about 65°, corresponding to the physically adsorbed water, was found in a sequence as 13.9% (γ-AlOOH)>12.5% (Ti–Al-10)>11.1% (Ti–Al-30)> 8.96% (Ti–Al-40). The excess water (13.9%) contained in γ-AlOOH sample was possibly obtained from gelation after the reaction as reported (Levin and Brandon 1998). Mass loss of titania nanocomposites at the first stage is well proportional to the fraction of boehmite, indicating that excess water is mainly contained in the boehmite phase. A further gradual loss of 13.6% appears at the temperature range from 150° to 480° due to boehmite dehydration, and a final loss of 2.2% is ascertained at a temperature from 480° to 700°, attributing to the trace amount of hydroxyl moiety retained in γ-Al_2O_3. As a result, for the γ-AlOOH case, total mass loss at a temperature from 150° to 700° was about 15.8%, which is in good agreement with theoretical value 15.02%. Du et al. have constructed blowball-like boehmite by chemical precipitation using $Al(NO_3)_3$ as a precursor at pH 7 and found around 29.1% mass loss in the temperature range from 150° to 495°, much larger than the theoretical mass loss of boehmite dehydration. They attributed it to the easily adsorbed water as hydration water in preparation (Du et al. 2009). However, the preparation in our experiments occurred in absolute ethanol and no excess absorbed water was observed

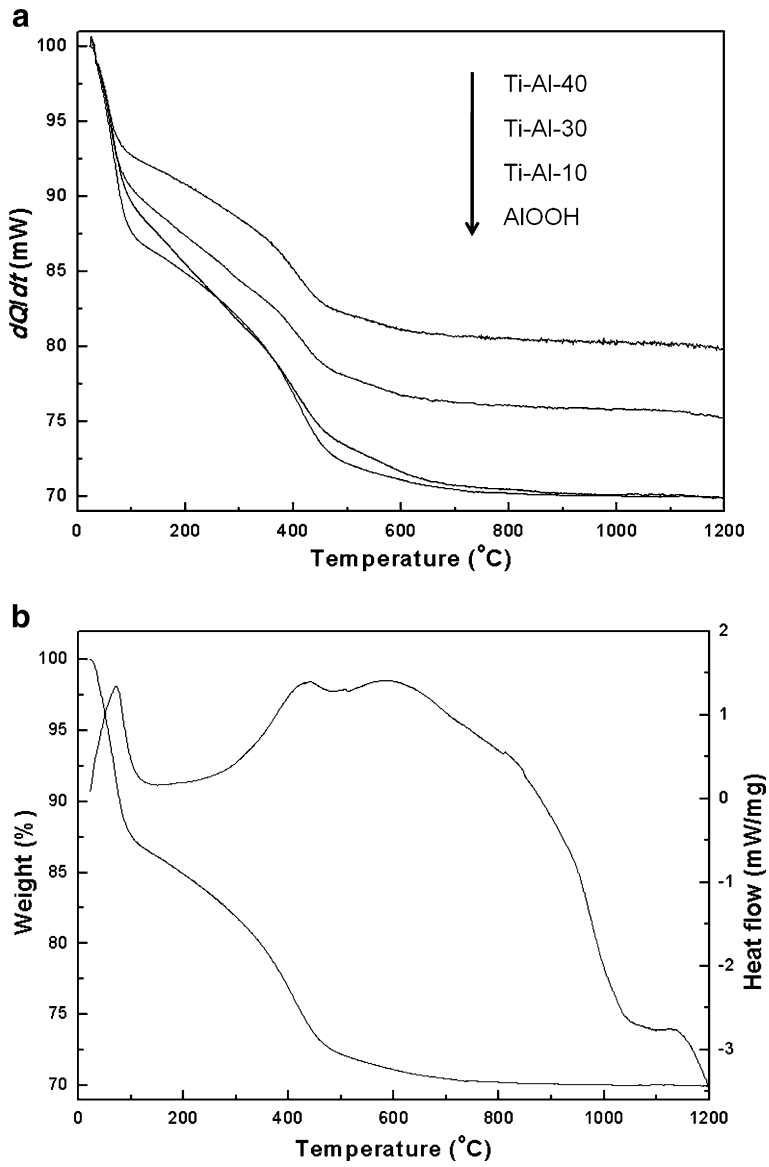

Fig. 3 TG-DSC analysis of Ti–Al series and γ-AlOOH. **a** TG analysis of Ti–Al series and γ-AlOOH. **b** TG-DSC analysis of γ-AlOOH

in mass loss. Similar observations are achieved for mass loss of Ti–Al composites.

3.4 Specific Surface Area Determination and SEM Observation

The microstructures of synthesized samples were further investigated using SEM analysis, as seen in Fig. 4. The morphology of γ-AlOOH under a similar synthetic procedure was reported as nanofibers (Park et al. 2007), and in our samples a fiber-like nanostructure was also recognized (shown to be labeled with an ellipse). There is no evident surface difference among the samples containing variable titania content, even the large clusters in Ti–Al-40 based on the observations of SEM images. The BET areas are summarized in Table 1. After introduction of 10 wt.% P25, the BET area of AlOOH was increased from 393 to 458 $m^2\ g^{-1}$. Further addition inversely decreased the BET area to 256 $m^2\ g^{-1}$ in sample Ti–Al-40. We propose that an appropriate amount of P25 added was uniformly dispersed into the aluminum

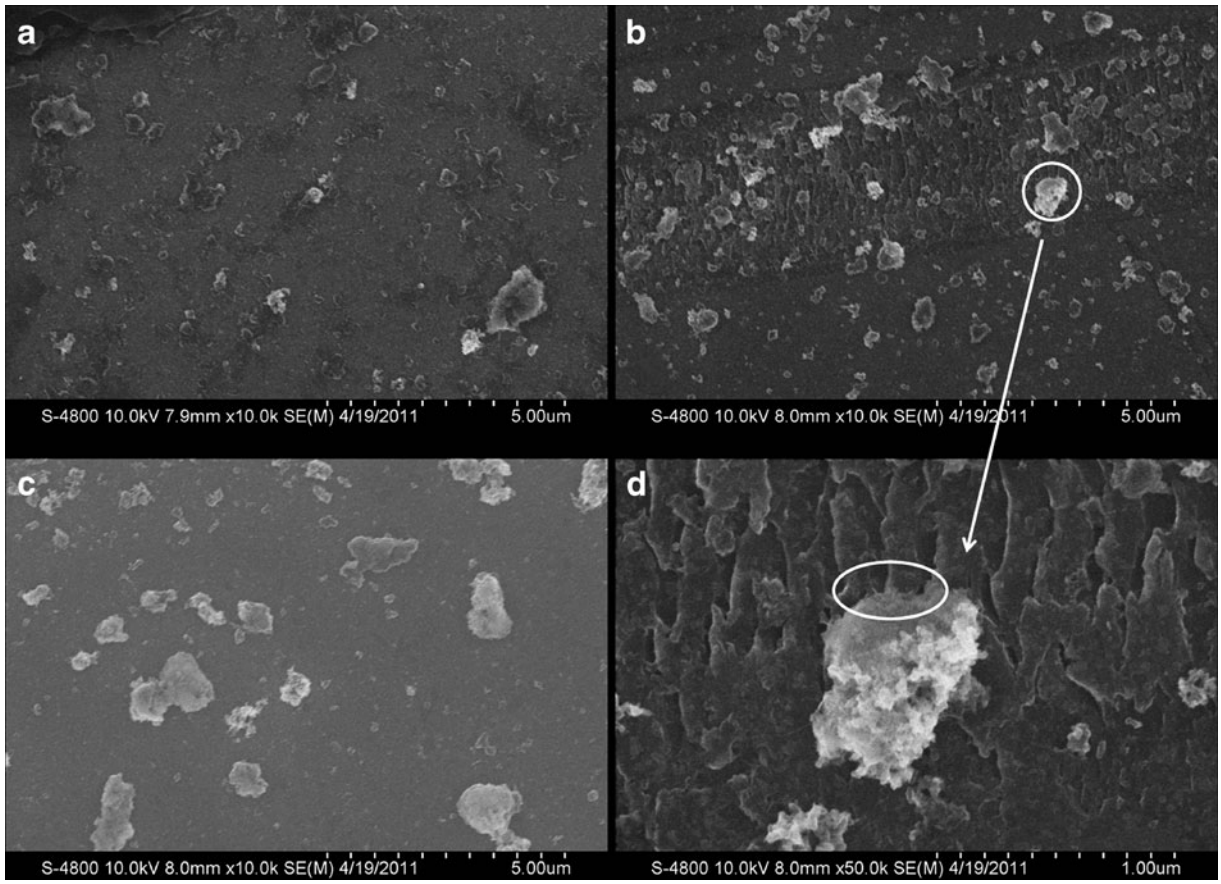

Fig. 4 SEM images of Ti–Al series (*A*, Ti–Al-10; *B*, Ti–Al-30; *C*, Ti–Al-40; *D*, a selected cluster from *B*)

matrix to form relatively small clusters, thus enhancing the BET area, and the excess amount of P25 in bulk, inversely, appears to form relatively large clusters, thus reducing the BET area, which is confirmed by the SEM images.

3.5 Photoreactivity Evaluation

Photocatalytic decolorization of MO molecules in aqueous medium was carried out in the presence of prepared titania nanocomposites, such as Ti–Al-10, Ti–Al-30, and Ti–Al-40 with the variation of irradiation time. Commercial titania P25 was evaluated under a similar condition for comparison purposes. The amounts of catalysts were chosen to achieve approximately the same quantity of TiO_2 loading. From Fig. 5, it is evident that decolorization efficiency is significantly enhanced in the light of the increase of TiO_2 content. After 130 min of irradiation, Ti–Al-40 was able to remove MO over 90%, while samples Ti–Al-30 and Ti–Al-10 could reduce around 85% and 70% MO substance, respectively. Pure P25 was the

Table 1 BET surface area of Ti–Al series and γ-AlOOH

	γ-AlOOH	Ti–Al-10	Ti–Al-30	Ti–Al-40
TiO_2 content (wt.%)	0	10	30	40
BET surface area (m^2/g)	393	458	312	256

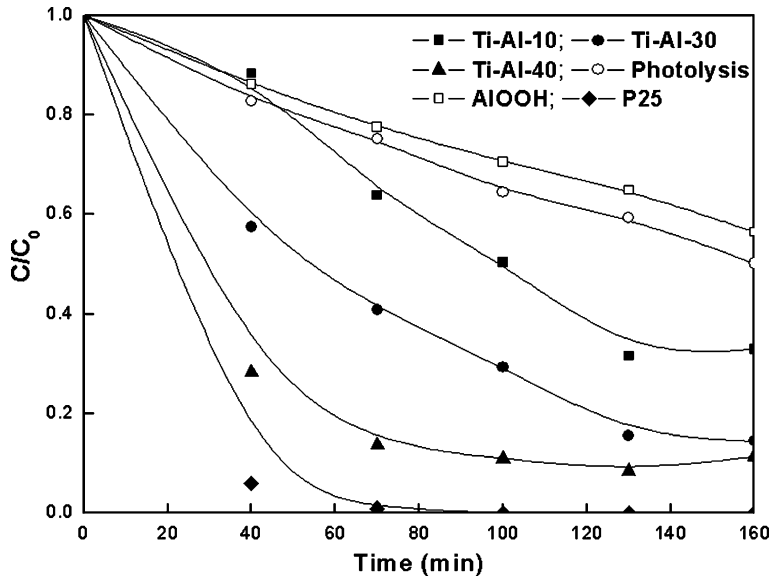

Fig. 5 Photocatalytic decolorization of MO versus irradiation time (initial concentration of MO, 10 mg/L; TiO_2 dosage, 0.5 g/L)

best candidate to reduce the organic compounds from aqueous media, even in a short reaction time. In our experiment, the titania surface was partially covered by the boehmite phase and the number of active sites was therefore reduced, causing the relatively low photocatalytic activity of the synthesized sample in comparison with pure P25. Based on the above observation, we adopted Ti–Al-40 as a photocatalyst for the following experiments with a fixed reaction time of 100 min.

The effect of catalyst dosage (Fig. 6) and initial concentrations (Fig. S2 of the "Electronic Supplementary Material") on the decolorization efficiency was subsequently determined. As seen in Fig. 6, the photocatalytic ability of titania-γ-AlOOH nanocomposites is reinforced with the increase of catalyst concentration from 0.1 to 0.25 g/L. Beyond that, the dye removal efficiency is inversely decreased when catalyst dosage is continuously improved. It is easily explained that, before optimal catalyst dosage, the increase of catalyst leads to augment the number of active sites, in turn enhancing the removal efficiency. However, the excess amount of catalyst decreases degradation by reason of interception of the light from the suspension. As a result, catalyst dosage of 0.25 g/L was picked for posterior tests. Low initial concentration of MO in an aqueous system was favorable to complete decomposition, which was in accordance with published reports (Akpan and Hameed 2009).

It is well known that the pH value in aqueous solutions makes a pivotal role during the photodegradation processes though the mechanisms proposed by different groups are still contradictory. In our study, a series of experiments underwent the pH range from 2 to about 10 while keeping the initial concentration at 10 mg/L constant. Satisfactory results were found for all entries even if the pH values were varied in Fig. 7. At low pH values, high decolorization of titania-γ-AlOOH catalysts is possibly due to the strong adsorption of MO, an anionic dye, onto the positively charged titania particles, hence facilitating the photocatalytic reactions. At pH>7, photodegradation is mainly influenced by two factors, the Coulombic repulsion between negatively quinoid-structured MO and TiO^- groups and the increased amount of hydroxyl radicals generated from the reaction between hydroxide ions and positive holes. The former factor decreases the decolorization while the latter one strengthens the photocatalytic avidity (Akpan and Hameed 2009). The latter factor might be dominant in our process on the basis of the achieved results.

Eventually, we attempted the recycling and durability of titania-γ-AlOOH composites. It is worth noting that synthesized catalysts could be simply

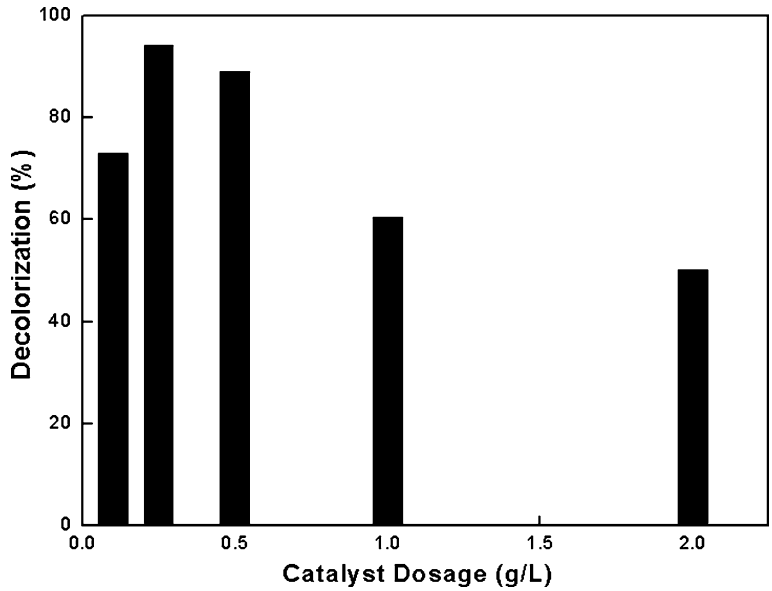

Fig. 6 Photocatalytic decolorization of MO versus catalyst dosage (initial concentration of MO, 10 mg/L; irradiation time, 100 min)

separated and regenerated using the procedure described in the "Experimental" section. The titania composites could be used at least six times for the photocatalytic decolorization of MO without any loss of activity.

4 Conclusion

We have prepared a series of titania-γ-AlOOH nanocomposites using a one-pot synthetic procedure and the samples were fully characterized by several techniques, such as FT-IR, XRD, SEM, TG-DSC, and N_2 physisorption analyses. Titania was successfully incorporated into the γ-AlOOH matrix and the photocatalytic activity of these samples was evaluated to remove MO substrate from aqueous media in the presence of UV irradiation. Several factors, which might affect the removal efficiency, such as irradiation time, pH values, initial concentration of MO, and catalyst dosage, were systematically investigated. Under optimum conditions, the catalyst could render

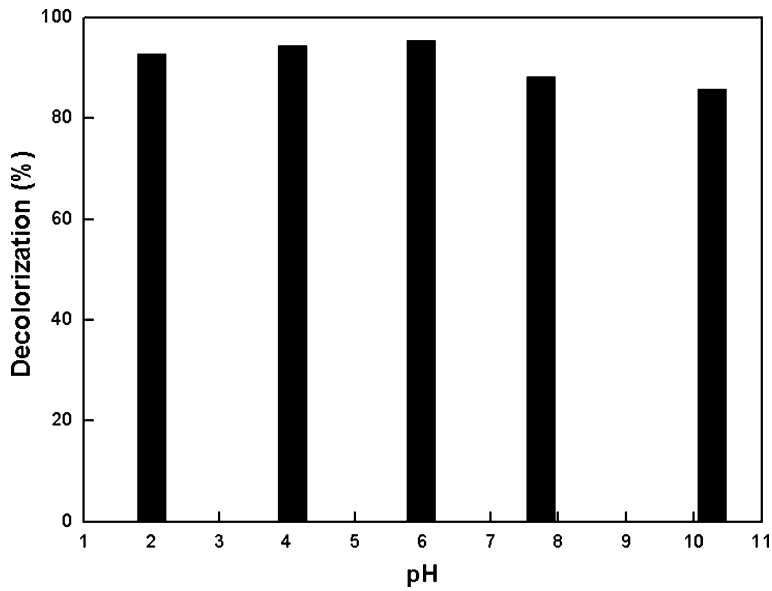

Fig. 7 Photocatalytic decolorization of MO versus pH values (initial concentration of MO, 10 mg/L; irradiation time, 100 min; TiO_2 dosage, 0.25 g/L)

complete decolorization of MO. Finally, the recoverable and reusable tests verified the durability of titania-γ-AlOOH nanocomposites.

Acknowledgments We are grateful of the financial supports from the Innovation Program of Shanghai Municipal Education Commission (11YZ113), the Special Research Fund in Shanghai Colleges and Universities to Select and Train Outstanding Young Teachers (slg10014), and the National Science Foundation of China (41076040 and 20807036).

References

Akpan, U. G., & Hameed, B. H. (2009). *Journal of Hazardous Material, 170*, 520.

Arami, H., Mazloumi, M., Khalifehzadeh, R., & Sadrnezhaad, S. K. (2008). *Journal of Alloys and Compounds, 461*, 551.

Caiut, J. M. A., Ghys, J. D., Kihn, Y., Verelst, M., Dexpert, H., Ribeiro, S. J. L., et al. (2009). *Powder Technology, 190*, 95.

Chang, F., Kim, H., Lee, B., Park, S., & Park, J. (2010). *Tetrahedron Letters, 51*, 4250.

Chiou, C. S., Shie, J. L., Chang, C. Y., Liu, C. C., & Chang, C. T. (2006). *Journal of Hazardous Material, 137*, 1123.

Chong, M. N., Jin, B., Chow, C. W. K., & Saint, C. (2010). *Water Research, 44*, 2997.

Du, X., Wang, Y., Su, X., & Li, J. (2009). *Powder Technology, 192*, 40.

Han, F., Kambala, V. S. R., Srinivasan, M., Rajarathnam, D., & Naidu, R. (2009). *Applied Catalysis A, 359*, 25.

Hochepied, J. F., & Nortier, P. (2002). *Powder Technology, 128*, 268–275.

Hoffmann, M. R., Martin, S. T., Choi, W., & Bahnemann, D. W. (1995). *Chemical Reviews, 95*, 69.

Jiang, G. D., Lin, Z. F., Chen, C., Zhu, L. H., Chang, Q., Wang, N., et al. (2011). *Carbon, 49*, 2693.

Kawasaki, N., Ogata, F., & Tominaga, H. (2010). *Journal of Hazardous Material, 181*, 574.

Leary, R., & Westwood, A. (2011). *Carbon, 49*, 741.

Levin, I., & Brandon, D. (1998). *Journal of the American Ceramic Society, 81*, 1995.

Liu, Y., Zhang, Y., Ge, C., Yin, H., Wang, A., Ren, M., et al. (2009). *Applied Surface Science, 255*, 7427.

Malato, S., Fernández-Ibáñez, P., Maldonado, M. I., Blanco, J., & Gernjak, W. (2009). *Catalysis Today, 147*, 1.

Panias, D., & Krestou, A. (2007). *Powder Technology, 175*, 163.

Park, I., Kwon, M., Kang, K., Lee, J., & Park, J. (2007). *Advanced Synthesis and Catalysis, 349*, 2039.

Petkowicz, D. I., Pergher, S. B. C., da Silva, C. D. S., da Rocha, Z. N., & dos Santos, J. H. Z. (2010). *Chemical Engineering Journal, 158*, 505.

Qiu, S., Xu, S. W., Ma, F., & Yang, J. X. (2011). *Powder Technology, 210*, 83.

Roco, M. C. (1999). *Journal Nanoparticle Research, 1*, 1.

Thompson, T. L., & Jr, J. T. (2006). Tates. *Chemical Reviews, 106*, 4428.

Yang, J., Frost, R. L., & Yuan, Y. (2009). *Thermochimica Acta, 483*, 29.

Zeng, J., Liu, S., Cai, J., & Zhang, L. (2010). *Journal of Physical Chemistry C, 114*, 7806.